Signal inhibition by a dynamically regulated pool of monophosphorylated MAPK

Michal J. Nagiec[a,b,*,†], Patrick C. McCarter[b,c,*], Joshua B. Kelley[a,b], Gauri Dixit[b,‡], Timothy C. Elston[a], and Henrik G. Dohlman[a,b]

[a]Department of Pharmacology, [b]Department of Biochemistry and Biophysics, and [c]Bioinformatics and Computational Biology, University of North Carolina at Chapel Hill, Chapel Hill, NC 27599

ABSTRACT **Protein kinases regulate a broad array of cellular processes and do so through the phosphorylation of one or more sites within a given substrate. Many protein kinases are themselves regulated through multisite phosphorylation, and the addition or removal of phosphates can occur in a sequential (processive) or a stepwise (distributive) manner. Here we measured the relative abundance of the monophosphorylated and dual-phosphorylated forms of Fus3, a member of the mitogen-activated protein kinase (MAPK) family in yeast. We found that upon activation with pheromone, a substantial proportion of Fus3 accumulates in the monophosphorylated state. Introduction of an additional copy of Fus3 lacking either phosphorylation site leads to dampened signaling. Conversely, cells lacking the dual-specificity phosphatase (*msg5*Δ) or that are deficient in docking to the MAPK-scaffold (Ste5ND) accumulate a greater proportion of dual-phosphorylated Fus3. The double mutant exhibits a synergistic, or "synthetic," supersensitivity to pheromone. Finally, we present a predictive computational model that combines MAPK scaffold and phosphatase activities and is sufficient to account for the observed MAPK profiles. These results indicate that the monophosphorylated and dual-phosphorylated forms of the MAPK act in opposition to one another. Moreover, they reveal a new mechanism by which the MAPK scaffold acts dynamically to regulate signaling.**

Monitoring Editor
Charles Boone
University of Toronto

Received: Jan 22, 2015
Revised: Jun 19, 2015
Accepted: Jul 8, 2015

INTRODUCTION

All cells must detect, interpret, and respond to a broad array of environmental signals. Most signal transduction pathways depend on the phosphorylation of cellular proteins by protein kinases. Among the best known are the mitogen-activated protein kinases (MAPKs), which are phosphorylated and activated by a MAPK kinase (MAPKK), which are in turn phosphorylated and activated by a MAPKK kinase (MAPKKK). These cascades respond to a variety of stress conditions and secreted hormones and are conserved in organisms ranging from yeast to humans.

The budding yeast *Saccharomyces cerevisiae* uses a typical MAPK signaling pathway to initiate the mating response. Haploid cells of the opposite mating type (**a**- or α-cells) secrete peptide pheromones that bind to cell surface receptors. These receptors activate a G protein and a protein kinase cascade comprising Ste11 (MAPKKK), Ste7 (MAPKK), and Fus3 (MAPK). All three of these kinases interact with the scaffold protein Ste5, which recruits the constituent kinases to the activated G protein at the plasma membrane. In addition to Fus3, a second MAPK Kss1 is activated by Ste7 but does not interact directly with Ste5. Thus, whereas Ste5 is required for activation of Fus3 (Breitkreutz *et al.*, 2001; Andersson *et al.*, 2004; Kusari *et al.*, 2004; Maleri *et al.*, 2004; Flatauer *et al.*, 2005), it binds poorly to Kss1 and is not required for Kss1-mediated processes (Choi *et al.*, 1994; Printen and Sprague, 1994; Kusari *et al.*, 2004). Once activated, Fus3 goes on to phosphorylate proteins

This article was published online ahead of print in MBoC in Press (http://www.molbiolcell.org/cgi/doi/10.1091/mbc.E15-01-0037) on July 15, 2015.

*These authors contributed equally.

Present addresses: †Department of Pharmacology, Weill Cornell Medical College, 1300 York Ave., New York, NY 10065; ‡Cellanyx Diagnostics, Beverly, MA 01915.

Address correspondence to: Henrik G. Dohlman (hdohlman@med.unc.edu), Timothy C. Elston (telston@amath.unc.edu).

Abbreviations used: BEM1, Bud EMergence 1; FUS3, cell FUSion 3; GFP, green fluorescent protein; G6PDH, glucose-6-phosphate dehydrogenase; KSS1, Kinase Suppressor of Sst2 mutations; MAPK, mitogen-activated protein kinase; MSG5, multicopy suppressor of GPA1; PTP, protein tyrosine phosphatase; SSD, sum of squared deviations; SST2, SuperSensiTive 2; STE, STErile; Thr, threonine; Tyr, tyrosine.

necessary for new gene transcription, cell division arrest, polarized cell expansion (chemotropic growth and shmoo formation), and cell–cell fusion (Wang and Dohlman, 2004). In the absence of Fus3, Kss1 can mediate the pheromone-dependent gene induction program (Roberts *et al.*, 2000; Breitkreutz *et al.*, 2001), whereas other responses, such as chemotropic growth, are abrogated (Hao *et al.*, 2008). Thus, although Fus3 and Kss1 are activated by the same upstream protein kinases, they have distinct cellular functions. Here our focus is on the function of Fus3 and its scaffold, Ste5.

Based on the specificity of binding, it was long assumed that Ste5 acts to direct signaling toward Fus3 and away from Kss1. Although clearly required for Fus3 activation, Ste5 does not prevent the activation of Kss1 by pheromone (Choi *et al.*, 1994; Printen and Sprague, 1994; Breitkreutz *et al.*, 2001; Andersson *et al.*, 2004; Maleri *et al.*, 2004; Flatauer *et al.*, 2005). It was later proposed that Ste5 is an allosteric regulator of Fus3. In support of that model, a fragment of Ste5 was demonstrated to promote Fus3 autophosphorylation at Tyr-182 (Bhattacharyya *et al.*, 2006), one of two sites normally phosphorylated upon full activation of the kinase (Gartner *et al.*, 1992). The monophosphorylated form of Fus3 was partially (20–25%) activated and competent to phosphorylate a variety of substrates in vitro (Bhattacharyya *et al.*, 2006).

If Ste5 were found to activate Fus3 in vivo, even partially, it would raise a host of new questions. What proportion of Fus3 is monophosphorylated in this manner? How does the pool of monophosphorylated kinase affect downstream signaling? Does autophosphorylation on one site facilitate or hinder subsequent phosphorylation at the second site? If autophosphorylation on one site were followed by a dissociation event and transphosphorylation on the second site, the scaffold might act to delay signaling. Alternatively, if the scaffold stabilizes the interaction of Ste7 and Fus3, phosphorylation might occur in a processive manner, without substrate dissociation and reassociation. This would have the effect of minimizing the monophosphorylated species and accelerating full activation of the MAPK (Ferrell, 2000; Levchenko *et al.*, 2000). Thus scaffold proteins could either speed or slow signal transduction, depending on the mechanism used.

Apart from altering the kinetics of MAPK activation, a processive or distributive mechanism could influence the dose–response relationship for the pathway. Theoretical and biochemical studies indicate that processive phosphorylation should favor a graded output, one that aligns MAPK activity with the graded input stimulus. Accordingly, scaffold proteins might convert an inherently switch-like MAPK to one that is more graded (Ferrell, 2000; Levchenko *et al.*, 2000). Conversely, distributive phosphorylation is believed to produce an all-or-none (switch-like) output (Huang and Ferrell, 1996). In support of this second model, a number of functional activity assays reveal that Ste5 is necessary for slow and ultrasensitive activation, as is observed for Fus3 but not Kss1 (Hao *et al.*, 2008; Malleshaiah *et al.*, 2010). Thus the distinction between processive and distributive phosphorylation has important implications for signal encoding (Piala *et al.*, 2014).

Considering the importance of how MAPKs are turned on and off, relatively little is known about how this occurs in cells. For example, it is still not established whether Ste5, or scaffolds in general, dictate a processive versus distributive phosphorylation mechanism in vivo. To address this question, we employ a new method to quantify the abundance of monophosphorylated and dual-phosphorylated Fus3 in the cell over time and in the presence or absence of Fus3 regulators; these regulators include the scaffold Ste5, as well as the MAPK phosphatases Ptp2, Ptp3, and Msg5. We show that Ste5 and Msg5 in particular act to limit full activation of Fus3 and that nearly half of the Fus3 pool remains nonphosphorylated after pathway stimulation. Of the protein that is phosphorylated, nearly half is in the monophosphorylated state. Whereas phosphorylation appears to be processive, dephosphorylation appears to be distributive. Finally, we show that monophosphorylated Fus3 does not activate, but instead impedes, the pheromone response in vivo. Together these findings indicate that the monophosphorylated species acts in a dynamic and dominant manner to limit signal transduction.

RESULTS

The phosphorylation state of Fus3 determines mating pathway output

It has long been recognized that MAP kinases must be phosphorylated on two residues in order to achieve full catalytic activity. This was originally documented for ERK2, for which the protein is phosphorylated on Tyr-185 and subsequently on the neighboring Thr-183 (Haystead *et al.*, 1992; Ferrell and Bhatt, 1997). This dual phosphorylation alters the conformation of the protein, thereby enabling ATP to bind to the catalytic site (Canagarajah *et al.*, 1997). These "activation loop" residues are conserved in the yeast ERK2 homologue Fus3, and mass spectrometry analysis indicates that the same order of events occurs (Hur *et al.*, 2008). Our goal here was to determine the relative abundance and potential function of the monophosphorylated MAPK species.

We began by constructing genomically integrated mutant forms of Fus3 that cannot be phosphorylated at either of the activation loop residues: Tyr-182, Thr-180, or both. We then monitored the transcription of a mating-specific gene reporter. As shown in Figure 1A, cells in which the endogenous *FUS3* gene had been deleted produced a maximal response to pheromone resembling the response of wild-type cells. In the absence of Fus3, pathway induction is preserved due to the action of a homologous MAPK, Kss1, as reported previously (Bardwell, 2005). In contrast, cells expressing a variant of Fus3 that can only be monophosphorylated ($Fus3^{T180A}$ or $Fus3^{Y182F}$) exhibited a substantially diminished response. This reduction in signal activity is particularly striking, given the near-normal response seen in the complete absence of Fus3 expression.

To determine whether the Fus3 mutants limit signaling via the primary (Fus3-mediated) pathway, we repeated these experiments but this time in cells that coexpress endogenous wild-type Fus3 and either an additional copy of the MAPK or one of the phosphosite mutants. As shown in Figure 1B, signaling was diminished most substantially in cells in which the second copy of Fus3 was mutated ($Fus3^{T180A}$ or $Fus3^{Y182F}$). Thus the monophosphorylated Fus3 dampens the mating response and does so in a genetically dominant manner. These findings suggest that the partially phosphorylated form of Fus3 acts to inhibit signaling.

The phosphorylation state of Fus3 is dynamically regulated

Having shown that monophosphorylated Fus3 inhibits the mating transcription response, we next sought to measure the relative abundance of the monophosphorylated protein in cells. To that end, we used the Phos-tag reagent. Phos-tag is a metal-coordinating small molecule with a high affinity for phosphorylated serine, threonine, and tyrosine (Kinoshita *et al.*, 2006). Addition of Phos-tag to acrylamide gels slows the migration of polypeptides and does so in proportion to the number of phosphorylations on the molecule. As shown in Figure 2A, the Phos-tag method revealed three species of Fus3 (corresponding to the dual-phosphorylated, monophosphorylated, and nonphosphorylated forms of the protein) after stimulation with 10 μM pheromone, a dose that produces full pathway

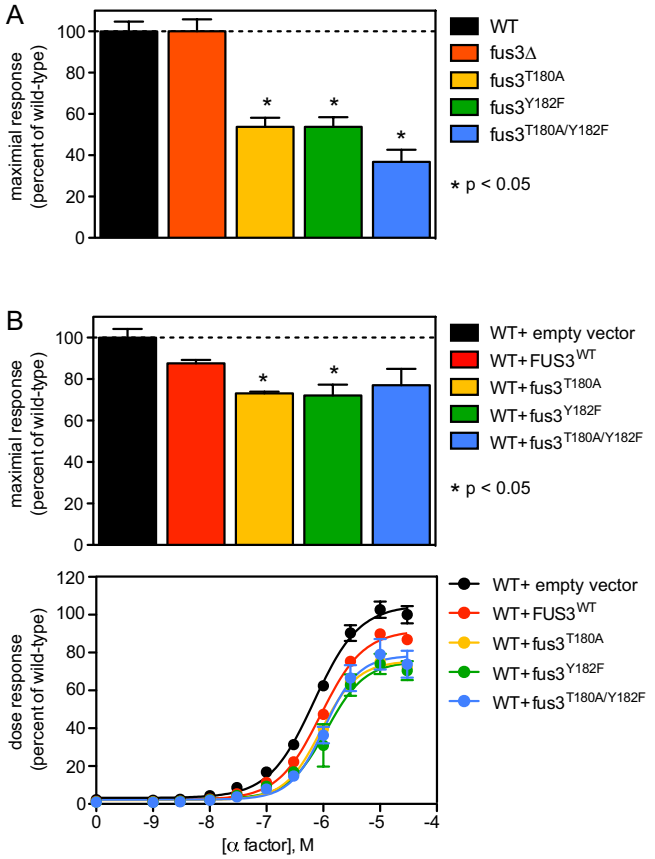

FIGURE 1: Signal inhibition by monophosphorylated Fus3. (A) Transcription reporter (FUS1-lacZ) activity in wild-type (WT), Fus3-deficient, or Fus3 activation loop mutant strains (*fus3*^{T180A}, *fus3*^{Y182F}, and combined *fus3*$^{T180A/Y182F}$) stimulated with 10 μM α-factor. (B) Same analysis in wild-type cells bearing a single-copy plasmid with no insert (vector), wild-type *FUS3*, or mutations in the Fus3 activation loop. FUS1-lacZ data are presented as a percentage of maximum activity in wild-type cells (A and B, top) and as a full dose–response curve (B, bottom). Results report ±SEM ($n = 3$) for each data point, but this is not visible in every case. *Statistically significant Student's *t* test of pairwise comparisons for wild type and the individual mutants.

activation (Figure 1B). As expected, the dual-phosphorylated form of Fus3 was enriched after pheromone treatment, but monophosphorylated Fus3 was still readily detectable. As a control, we established that the individual phosphosite mutants yielded just two bands each, corresponding to the monophosphorylated and nonphosphorylated species (Figure 2B). Whereas the pool of monophosphorylated species was enriched in these mutants, the proportion of nonphosphorylated protein was unaffected (Figure 2B). The Fus3^{Y182F} mutant migrated anomalously, equivalent to that of the activated wild-type form of the protein. In each case, only the slower-migrating phosphorylated species was evident using p44/p42 antibodies raised against a phosphorylated MAPK peptide. None of the phosphorylated species was detected in the absence of the upstream MAPK kinase Ste11 (Figure 2A). No bands were detected in a *FUS3*-deficient strain (Figure 2B).

Ste5 is believed to act in part by stimulating the autophosphorylation of Fus3 on Tyr-182 (Bhattacharyya *et al.*, 2006). Support for this model comes from in vitro studies using a peptide fragment of Ste5 (Bhattacharyya *et al.*, 2006). To determine whether Fus3 is also autophosphorylated in vivo, we compared the mobility of wild-type Fus3 and a catalytically inactive form of the protein (Fus3^{K42R}). As shown in Figure 2C, Fus3^{K54R} is monophosphorylated despite the lack of catalytic activity; as with the wild-type protein, the monophosphorylated species was evident in unstimulated conditions and increased further upon pheromone stimulation. Thus autophosphorylation is not the only means by which Fus3 becomes monophosphorylated and activated, at least in vivo. To determine the contribution of the scaffold Ste5, we monitored Fus3 in the absence of Ste5–Fus3 interaction. Deletion of *STE5* blocks signaling altogether, so as an alternative, we used a mutant form of Ste5 in which Fus3 docking is disrupted ("nondocking" allele, Ste5ND). This mutant binds poorly to Fus3 (Bhattacharyya *et al.*, 2006; Maeder *et al.*, 2007) and yet produces a transcription-induction response that is actually enhanced (Bhattacharyya *et al.*, 2006). Once again we were able to detect monophosphorylated Fus3 and at levels comparable to that of wild-type (*STE5*$^{+}$) cells. However, the relative abundance of dual-phosphorylated Fus3 was increased (~50%) in the Ste5ND strain compared with wild type (Figure 2C). This confirms previous observations that Ste5 does not activate but instead limits the full activation of Fus3 in vivo (Bhattacharyya *et al.*, 2006; Hao *et al.*, 2008). We infer that Ste5 acts in two opposing ways to regulate Fus3 activity. First, Ste5 binds to Fus3 indirectly via Ste7, thereby promoting activation. This is based on the observation that Fus3 binds poorly to Ste5ND but is nevertheless activated by Ste7. Second, Ste5 binds to Fus3 directly and inhibits activation. This is based on the enhanced signaling observed in Ste5ND cells.

Although Fus3 is phosphorylated by Ste7, Fus3 is also regulated by protein phosphatases. Accordingly, the cellular pool of monophosphorylated Fus3 is likely to be regulated through the combined action of kinases and phosphatases. To test this, we examined Fus3 in a panel of mutants lacking one or more of the known MAPK phosphatases: Ptp2 and Ptp3, which are Tyr-specific phosphatases, and Msg5, which is a dual-specificity (Tyr; Ser or Thr) phosphatase (Doi *et al.*, 1994; Zhan *et al.*, 1997; Remenyi *et al.*, 2005). As shown in Figure 2D, cells lacking the dual-specificity phosphatase (*msg5*Δ) exhibited a decrease in monophosphorylated Fus3. Cells lacking the Tyr-specific phosphatases exhibited an increase in basal levels of dual-phosphorylated Fus3, but there was little or no effect of these mutants in pheromone-stimulated cells (Figure 2D). These data suggest that Fus3 is dephosphorylated by Msg5 to enrich the cellular pool of monophosphorylated Fus3.

Ste5 and Msg5 regulate the kinetics of Fus3 phosphorylation

To expand our analysis, we next examined how the relative abundance of the monophosphorylated and dual-phosphorylated forms of Fus3 change over time. As shown in Figure 3A, pheromone-activated cells exhibited a substantial (~60%) drop in nonphosphorylated kinase within 5 min, accompanied by a corresponding increase in both the monophosphorylated and dual-phosphorylated forms of the protein. Whereas the pool of dual-phosphorylated Fus3 rose rapidly and showed an initial peak at ~2–3 min, the pool of monophosphorylated Fus3 rose in a more gradual manner. Most strikingly, the relative abundance of monophosphorylated and dual-phosphorylated Fus3 was nearly equivalent after the initial peak of activation (from 5 to 60 min). Taken together, these data establish that a substantial proportion of Fus3 exists in the monophosphorylated state. Together with the data presented earlier (Figure 1), these findings suggest that stimulated cells produce a combination of Fus3 that is fully phosphorylated (activated), monophosphorylated, and nonphosphorylated (inhibitory).

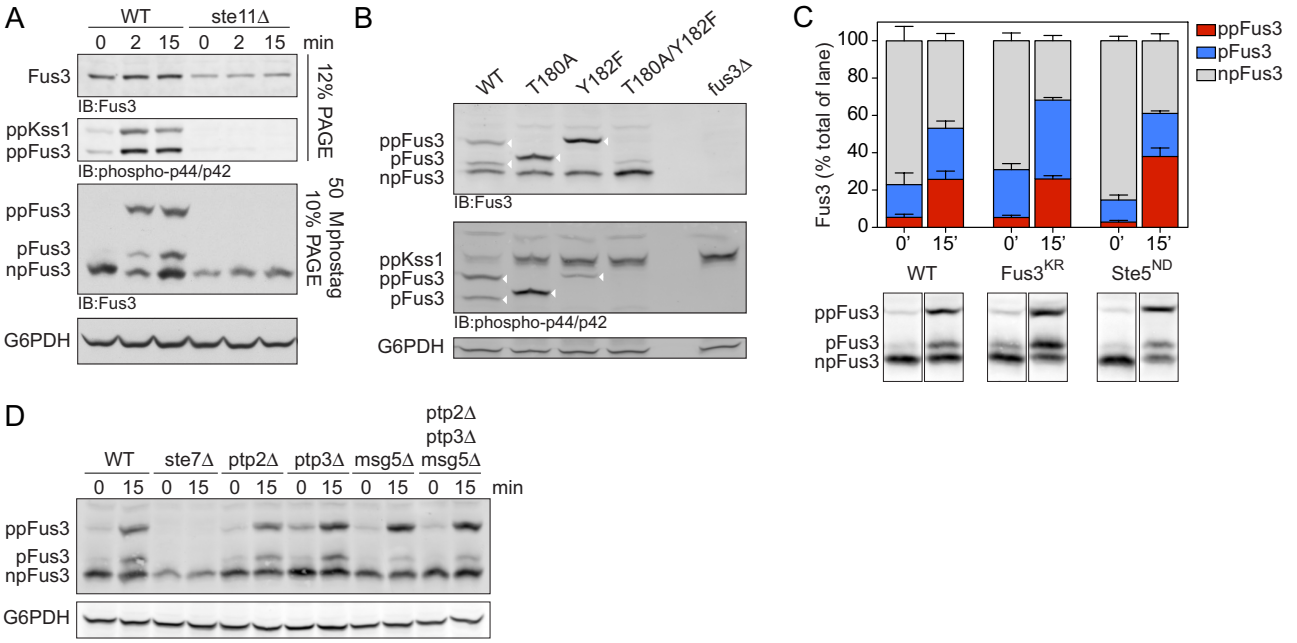

FIGURE 2: Analysis of differentially phosphorylated forms of Fus3. (A) Wild-type or *ste11*Δ (MAPKK) mutant cells untreated (0) or treated for 2 or 15 min with 10 μM α-factor were lysed and resolved by immunoblotting after SDS–PAGE and probed with Fus3 antibodies (top) or p44/p42 antibodies (top middle), with Phos-tag reagent and probed with Fus3 antibodies (bottom middle), or with G6PDH load control antibodies (bottom). Bands represent the dual-phosphorylated (ppKss1, ppFus3), monophosphorylated (pFus3), nonphosphorylated (npFus3), and total (Fus3) protein. Except for the topmost panel, this and all subsequent experiments were done using Phos-tag. (B) Wild-type, Fus3 activation loop (T180A, Y182F), and *fus3*Δ mutants were resolved by Phos-tag SDS–PAGE and immunoblotting with Fus3 antibodies (top), p44/p42 antibodies (middle), or G6PDH load control antibodies (bottom). Arrowheads indicate the bands of interest (i.e., those recognized by p44/42 antibodies). (C) Wild-type, *fus3*^{KR} (catalytically inactive), and *ste5*ND (nondocking) mutants untreated or treated for 15 min with 10 μM α-factor were resolved by Phos-tag SDS–PAGE and immunoblotted with Fus3 antibodies. Representative data are shown below. Band intensity was quantified as a percentage of total Fus3 in each lane. Results are reported as ±SEM ($n \geq 3$). (D) Wild-type, *ste7*Δ, and phosphatase-deficient *ptp2*Δ, *ptp3*Δ, and *msg5*Δ mutants, alone or in combination, were resolved by Phos-tag SDS–PAGE and immunoblotted with Fus3 antibodies (top) or G6PDH load control antibodies (bottom).

To further establish the long-term consequences of differential phosphorylation, we monitored Fus3 in cells lacking the protein phosphatases or that express mutant forms of the scaffold Ste5. As noted earlier, Ste5ND cannot dock to Fus3 but nevertheless allows activation of Fus3 by the upstream kinase Ste7. Compared with wild type, the Ste5ND mutant cells exhibited higher overall accumulation of dual-phosphorylated Fus3 (Figure 3B). In addition, we tested another variant of the scaffold (Ste5^{FB}), one that cannot undergo feedback phosphorylation and binds poorly to Fus3 (Malleshaiah *et al.*, 2010). As with the Ste5ND mutant, the Ste5^{FB} mutant exhibited higher accumulation of dual-phosphorylated Fus3 (Figure 3B), and this accumulation occurred more rapidly than in either the wild-type or Ste5ND strain. Thus binding to Ste5 or feedback phosphorylation of Ste5 limits the activation of Fus3 (Bhattacharyya *et al.*, 2006; Malleshaiah *et al.*, 2010). When binding or feedback is blocked, a greater proportion of Fus3 is fully activated. Given our goal of understanding the scaffolding function, we did all subsequent experiments with Ste5ND.

There are at least two ways by which Ste5 could impede Fus3 activation. One possibility is that Ste5 slows phosphorylation of Fus3 by the upstream MAPK kinase, Ste7. In support of this model, Ste5 was shown to impart some distinctive time- and dose-dependent behaviors to Fus3. Compared with Kss1, Fus3 is phosphorylated more slowly and in a more ultrasensitive manner (Hao *et al.*, 2008; Malleshaiah *et al.*, 2010). In the absence of docking to Ste5, Fus3 behaves like Kss1 (Hao *et al.*, 2008). Another possibility is that Ste5 accelerates dephosphorylation, perhaps by recruiting one or more MAPK phosphatases. As compared with wild type, cells lacking the dual-specificity phosphatase (*msg5*Δ) exhibited more rapid accumulation of dual-phosphorylated Fus3, although the differences narrowed after 60 min (Figure 3C). In contrast, there was no effect of deleting *PTP2* and *PTP3*. We infer that both Ste5 and Msg5 slow the accumulation of dual-phosphorylated Fus3.

Ste5 and Msg5 cooperate to maintain a pool of monophosphorylated Fus3

To further investigate the role of Ste5 in limiting Fus3 activity, we measured the accumulation of monophosphorylated versus dual-phosphorylated Fus3 in wild-type cells, in cells in which the interaction between Fus3 and Ste5 had been disrupted (*ste5*ND), and in cells lacking the phosphatase Msg5 (*msg5*Δ). For these experiments, we focused on early times and monitored the relative kinetics of Fus3 mono phosphorylation and dual phosphorylation. Compared with wild type, the peak of dual-phosphorylated Fus3 was more pronounced in the *ste5*ND mutant, but the monophosphorylated species remained roughly unchanged (Figure 4A, compare top left and right). In the *msg5*Δ strain, dual-phosphorylated Fus3 was again elevated, and in this case, the monophosphorylated pool

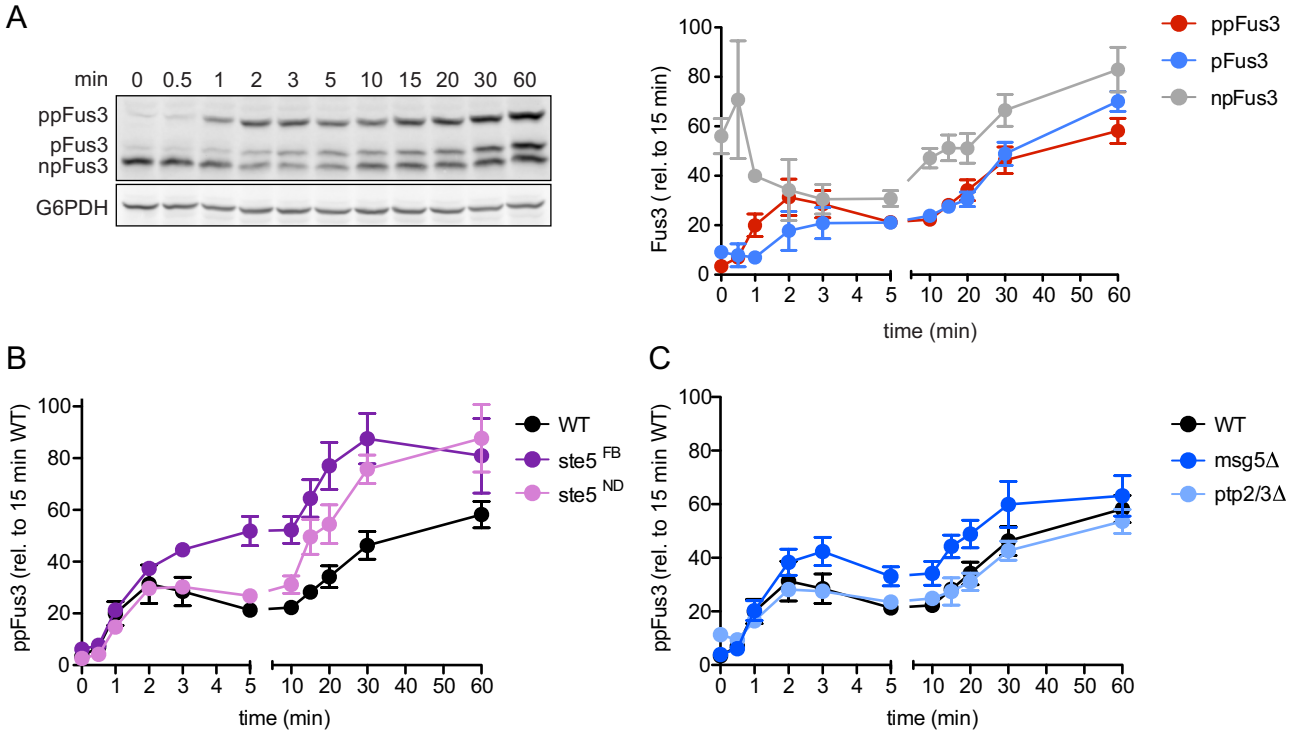

FIGURE 3: Dynamics of differentially phosphorylated forms of Fus3. (A) Left, wild-type cells were treated for the indicated times with 10 μM α-factor and resolved by Phos-tag SDS–PAGE and immunoblotted with Fus3 antibodies (top) or G6PDH load control antibodies (bottom). Right, dual-phosphorylated (ppFus3), monophosphorylated (pFus3), and nonphosphorylated (npFus3) quantified as a percentage of total Fus3 at 15 min. Results are reported as ±SEM ($n \geq 3$). (B and C) Wild-type (WT), *ste5*^{FB} (feedback-phosphorylation deficient), *ste5*ND (nondocking), *ptp2*Δ/ *ptp3*Δ, and *msg5*Δ (phosphatase-deficient) mutants treated and resolved by Phos-tag SDS–PAGE, as described. Dual-phosphorylated Fus3 is quantified as a percentage of total Fus3 at 15 min. Results are reported as ±SEM ($n \geq 3$).

of Fus3 was significantly diminished (Figures 4A, bottom left). These results are consistent with the view that both Ste5 and Msg5 limit the activity of Fus3. In contrast, a *ptp2/3*Δ double-deletion strain showed only small changes in the kinetics of monophosphorylated or dual-phosphorylated Fus3 (Figure 4A, bottom right).

In every case, the appearance of the dual-phosphorylated form of Fus3 preceded that of the monophosphorylated form. Although we can envision several mechanisms to account for this behavior, the simplest invokes processive phosphorylation and distributive dephosphorylation. To determine whether a distributive dephosphorylation mechanism can account for our experimental results and to quantify the relative roles of Ste5 and Msg5 in limiting MAPK activity, we developed three mathematical models to describe the kinetics of Fus3 activation and inactivation (Figure 4B). All of our models started with the pheromone-dependent recruitment of Ste5 to the plasma membrane. We did not explicitly model the activation of the kinases Ste11 and Ste7 but instead assumed a single rate-limiting step in the activation (dual phosphorylation) and recruitment of Fus3. Dephosphorylation of Fus3 was assumed to occur in a distributive manner. The abundances of Ste5, Ptp2, and Ptp3 were assumed to remain constant, whereas the production of Fus3 and Msg5 was assumed to increase as a function of Fus3 activity (feedback through gene induction).

Although our results and previous studies demonstrate that Ste5 dampens Fus3 activity, they do not establish a mechanism for this effect. Therefore we developed three models to test various scenarios for the mechanism by which feedback phosphorylation of Ste5 by Fus3 limits Fus3 activity. In the first scenario, feedback phosphorylation of Ste5 reduces the rate at which Fus3 is phosphorylated. In the second scenario, feedback phosphorylation of Ste5 increases the rate at which Fus3 is dephosphorylated (perhaps by recruiting a phosphatase). We tested each mechanism alone or in combination (third scenario).

The model equations (see *Materials and Methods*) were simulated using the NDSolve function in Wolfram Mathematica 9.0. To perform parameter estimations, we implemented a Markov chain Monte Carlo algorithm (Hao *et al.*, 2012) to search parameter space for sets of model parameter values that minimize the "aggregated" sum of squared deviations (SSDs) between experimental time courses for nonphosphorylated (npFus3), monophosphorylated (pFus3), and dual-phosphorylated (ppFus3) protein, as measured in wild-type, *ste5*ND, *msg5*Δ, and *ptp2/3*Δ cells. Surprisingly, models that include increased Fus3 dephosphorylation generated the best fits to the experimental data (Figure 4B, top right) and accurately captured the individual contributions of both Ste5 and Msg5 to signal dampening (Figure 4A). Thus the models suggest that the primary mechanism by which Ste5 limits Fus3 activity is by increasing the rate of dephosphorylation, potentially by recruiting a phosphatase.

To further confirm our assumption that phosphorylation occurs through a processive mechanism and dephosphorylation follows distributive kinetics, we tested a model that allowed for the possibility of a distributive (sequential) mechanism for Fus3 phosphorylation. However, to generate a good fit to the data, this model required that the second phosphorylation event occur substantially faster (by three orders of magnitude) than the first phosphorylation

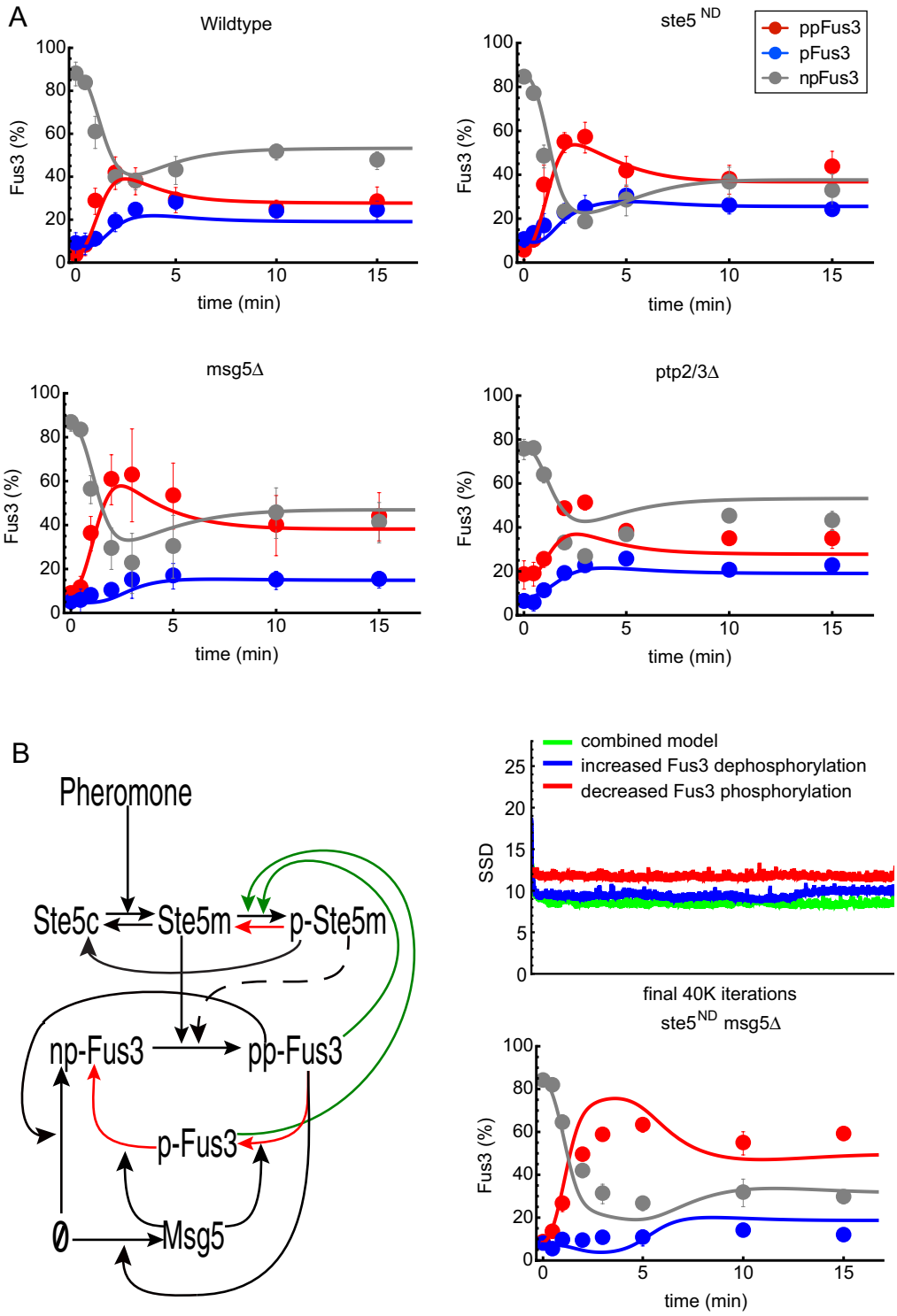

FIGURE 4: Dynamics and mathematical model of the differentially phosphorylated forms of Fus3. (A) Time series for wild-type (top left), *ste5*ND (nondocking) mutant (top right), *msg5*Δ (bottom left), and *ptp2*Δ/*ptp3*Δ (bottom right) cells treated with 10 μM α-factor and resolved by Phos-tag SDS–PAGE and immunoblotting with Fus3 antibodies. Dual-phosphorylated (ppFus3), monophosphorylated (pFus3), and nonphosphorylated (npFus3) quantified as a percentage of total Fus3. Results are reported as ±SEM ($n \geq 3$). Circles are experimental results. Lines are simulation results of the mathematical model shown in B. (B) Left, diagram of the mathematical models. Black lines represent pathway components present in all models. The dashed line is included in the model in which feedback-phosphorylated Ste5 (pSte5) limits Fus3 phosphorylation (activation), and the red lines are included in the model in which feedback-phosphorylated Ste5 increases Fus3 dephosphorylation (deactivation). The combined model includes both effects. Top right, performance of all three models. This graph shows values for the sum of squared deviations (SSDs) for the 39,000 best parameter sets found by the Monte Carlo algorithm for parameter estimation. Bottom right, model predictions for the combined model and corresponding experimental results for the *ste5*ND *msg5*Δ double mutant.

event. Thus this model effectively reduced to a processive (single-step) mechanism, validating our use of a processive phosphorylation model.

Loss of a phosphatase and MAPK scaffolding confers synthetic supersensitivity to pheromone

To test the validity of the models, we used each model to predict Fus3 activity in a strain containing the nondocking Ste5 mutant and also lacking Msg5 (*ste5*ND *msg5*Δ). Of interest, the models in which Fus3 dephosphorylation is increased by feedback phosphorylation to Ste5 predicted that the double-mutant strain would accumulate substantially more dual-phosphorylated Fus3 than either of the single mutants alone (Figure 4B, bottom right). Experimental measurements made in the double mutant showed excellent agreement with these model predictions (Figures 4B, bottom right, and 5A). At the level of transcription, the effects of the double mutant were similarly magnified (Figure 5B). Whereas the individual mutants conferred approximately twofold decrease in the EC_{50} for pheromone, combining the two mutations resulted in greater than eightfold decrease in EC_{50}. This increase in pheromone sensitivity is in marked contrast to the reduction in transcription activation presented in Figure 1, in which accumulation of monophosphorylated Fus3 dampened the transcription response by up to 60%, depending on the genetic background. These opposing effects on activity are qualitatively similar to those exhibited by the "benchmark" pathway regulator, the GTPase- activating protein Sst2. Whereas deletion of *SST2* confers a decrease in the EC_{50}, twofold overexpression of *SST2* dampens the maximum response (Hao *et al.*, 2003). Collectively these data support the predictions of the model and indicate that Ste5 and Msg5 cooperate to limit the accumulation of fully phosphorylated Fus3.

Finally, we considered the role of Ste5 and Msg5 in the mating response. When exposed to high concentrations of mating pheromone, yeast cells will arrest in G1 and expand in a polarized manner. Cells lacking Sst2 arrest at concentrations much lower than that needed by wild-type cells (Chan and Otte, 1982a,b) and do not polarize properly (Segall, 1993). In addition, we found that cells bearing the *msg5*Δ and *ste5*ND mutations exhibited a greater sensitivity to pheromone in the growth arrest plate assay (Figure 5C). To monitor cell polarization, we used a custom-designed microfluidic device and tracked the distribution of Bem1–green fluorescent protein (GFP) as a marker of the polar cap (Dixit *et al.*, 2014; Kelley *et al.*, 2015). Whereas wild-type and *msg5*Δ cells polarized quickly and expanded in a single direction, *ste5*ND and *msg5*Δ *ste5*ND strains turned frequently and failed to orient in any one direction (Figure 5D). Thus the *ste5*ND *msg5*Δ strain exhibits transcription and polarization defects similar to those reported previously for *sst2*Δ. Whereas Sst2 limits activation of both Fus3 and Kss1, Ste5 and Msg5 act specifically to limit the accumulation of dual-phosphorylated Fus3.

DISCUSSION

It is well known that MAPKs are dually phosphorylated and activated in response to an extracellular signal. Here we demonstrate that Fus3 is both monophosphorylated and dually phosphorylated in response to pheromone stimulation. The dual-phosphorylated species accumulates rapidly and precedes the appearance of the monophosphorylated species, suggesting a processive mechanism of phosphorylation and a distributive mechanism of dephosphorylation. The scaffold Ste5 and the phosphatase Msg5 act together to maintain a substantial pool of monophosphorylated Fus3. Monophosphorylated Fus3 appears to be a functionally important protein species, one that inhibits signal transmission and does so in a functionally dominant manner.

Previous studies demonstrated that Ste5 and Ste7 compete for binding with Fus3, and, in such a case, there would have to be a dissociation event between steps of autophosphorylation (Ste5–Fus3) and transphosphorylation (Ste7–Fus3; Kusari *et al.*, 2004). Thus, on the basis of the literature, we expected to observe distributive phosphorylation of Fus3. Moreover, a distributive mechanism had already been demonstrated for extracellular signal-regulated kinase (ERK) in vitro (Haystead *et al.*, 1992; Ferrell and Bhatt, 1997). A more recent analysis, however, revealed that ERK is phosphorylated processively in cells (Aoki *et al.*, 2011). As with Fus3, the monophosphorylated species of ERK does not precede but instead accompanies the appearance of the dual-phosphorylated species (Aoki *et al.*, 2011). These differences suggest that there are additional proteins or processes in the cell that modulate MAPK phosphorylation in vivo. According to one model, the effects of molecular crowding, as exists in the cellular milieu, accelerate MAPK activation so as to appear processive in vivo. In support of that model, investigators showed that the addition of an osmolyte (to displace water and mimic the effects of molecular crowding) conferred a processive rate of activation in vitro (Aoki *et al.*, 2011). Molecular crowding could just as easily be achieved by binding to scaffolds such as Ste5 or Pbs2 in yeast and kinase suppressor of Ras (KSR) or c-Jun N-terminal kinase inhibitory protein (JIP) in animals (Breitkreutz and Tyers, 2006). Pbs2 serves as both a scaffold and a MAPKK for the p38 orthologue Hog1, which, like Fus3 is phosphorylated in a processive manner in vivo (English *et al.*, 2015). In this way, scaffolds might act to increase the thermodynamic activity, and thereby promote phosphorylation, of the kinase.

Another consideration is the effect of protein localization. Whereas activated MAPKs typically translocate into the nucleus, where they phosphorylate transcription regulators, other substrates are located at the plasma membrane or in the cytoplasm. For example, Fus3 directly phosphorylates the nuclear transcription factor Ste12 (Elion *et al.*, 1993; Hung *et al.*, 1997; Breitkreutz *et al.*, 2001), as well as the cytoplasmic protein Sst2 (Garrison *et al.*, 1999; Parnell *et al.*, 2005). Moreover, subcellular localization is highly dynamic. Under conditions in which Fus3 translocates from the plasma membrane to the nucleus, Ste5 shuttles from the nucleus to the plasma membrane (Mahanty *et al.*, 1999; van Drogen *et al.*, 2001; Maeder *et al.*, 2007). These movements are likely to affect local concentrations of enzyme, scaffold, and substrate and consequently affect signal output. For instance, when Ste5 is permanently tethered to the plasma membrane, the transcriptional output is more graded than it is in wild-type cells (Takahashi and Pryciak, 2008). Thus changes in scaffold binding, concentration, and localization can all have potentially important effects on signal output.

Given the difficulty of reconciling MAPK activities in vivo and in vitro, we took an alternative approach in silico. Specifically, we built a computational model in which Fus3 is phosphorylated processively and dephosphorylation depends on feedback interactions with the scaffold and phosphatases. Our model also posits that feedback phosphorylation of Ste5 slows the rate of downstream signaling and protects against signal saturation. We have shown experimentally that Ste5 cooperates with Msg5 to maintain the pool of monophosphorylated Fus3. Msg5 could be acting directly on Fus3 or indirectly through Ste5 or a Ste5-binding partner (Remenyi *et al.*, 2005). Ste5ND on its own has little effect on the abundance of monophosphorylated Fus3. When interactions with both Ste5 and Msg5 are disrupted, however, nearly all of the Fus3 protein is dually phosphorylated. Fus3 and Ste5 also regulate the abundance of Msg5

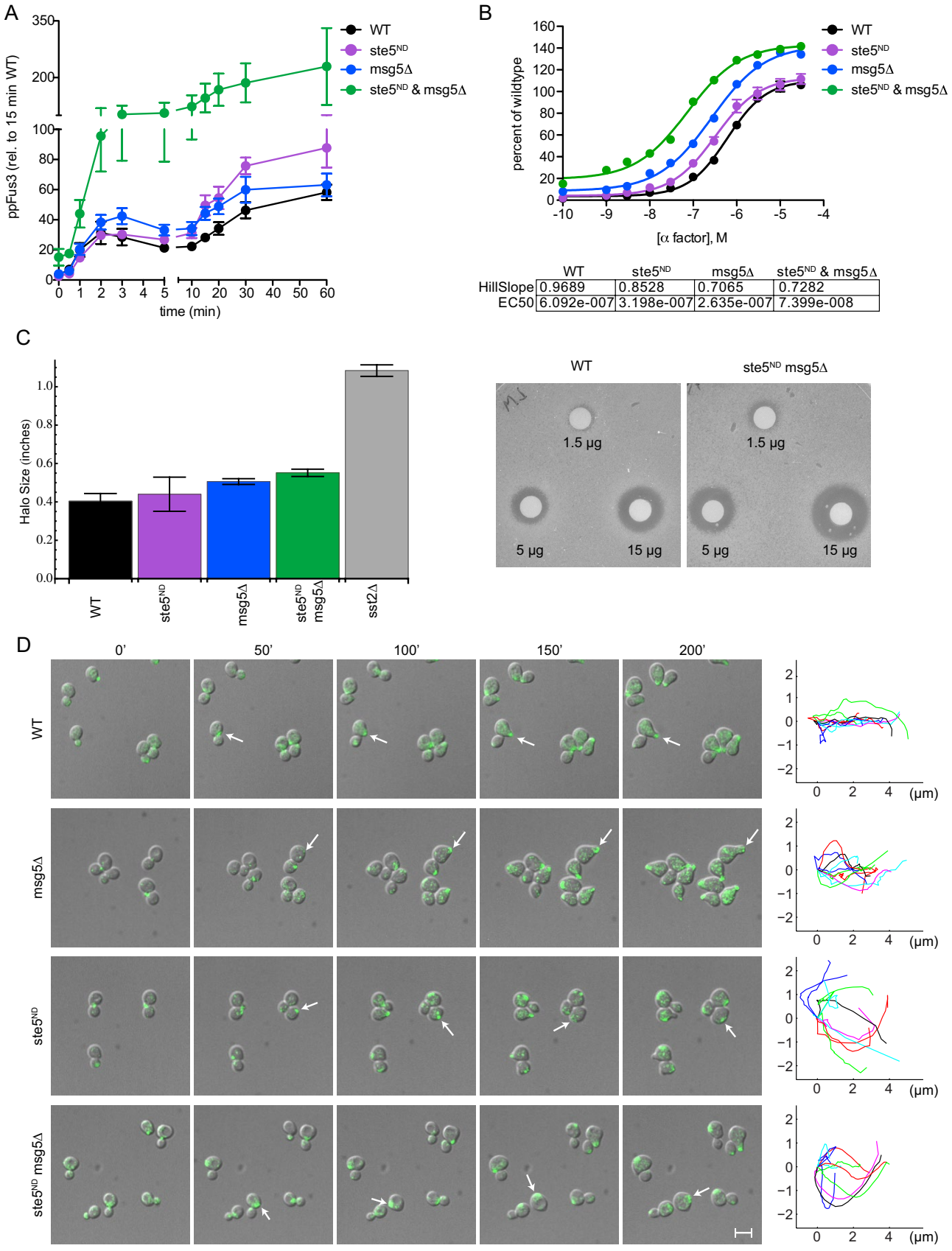

	WT	ste5ND	msg5Δ	ste5ND & msg5Δ
HillSlope	0.9689	0.8528	0.7065	0.7282
EC50	6.092e-007	3.198e-007	2.635e-007	7.399e-008

FIGURE 5: Synergistic activation of Fus3. (A) Dual-phosphorylated Fus3 in wild type and *ste5*ND (nondocking) *msg5*Δ (phosphatase-deficient) mutants replotted from Figure 3 for comparison with the *ste5*ND *msg5*Δ mutant. Dual-phosphorylated Fus3 is quantified as a percentage of total Fus3 at 15 min. Results are reported as ±SEM ($n \geq 3$). (B) Transcription reporter data in the same strains as in A, as a percentage of maximum activity in wild type. Inset, Hill

through gene induction, thereby providing another mechanism to fine-tune MAPK activity over time. Independently, these mechanisms dynamically regulate Fus3 phosphorylation. Collectively these mechanisms generate a dynamic self-regulatory network. Whereas Fus3 is partially redundant with the MAPK Kss1, Kss1 does not bind to Ste5 and was not considered in this analysis.

Our findings add support to the proposal that monophosphorylated Fus3 down-regulates pathway activity and does so through phosphorylation of Ste5 (Bhattacharyya *et al.*, 2006; Hao *et al.*, 2008; Malleshaiah *et al.*, 2010). Further, our data provide evidence that autophosphorylation is a minor contributor to the pool of monophosphorylated Fus3. Although our data point to the importance of Msg5 and dephosphorylation in this process, other (as-yet-unidentified) mechanisms may further contribute to the production of monophosphorylated Fus3 in vivo.

Collectively our findings reveal a substantial pool of nonphosphorylated and monophosphorylated Fus3 in pheromone-stimulated cells, and these have an inhibitory effect on signaling. This could account for the ability of a second copy of Fus3 to partially dampen the activity of the mating pathway. Although we do not know the mechanism of inhibition in this case, there is growing evidence that even catalytically inactive kinases can have important cellular functions. Approximately 10% of all human kinase genes lack one of three key residues necessary for activity and are therefore likely to be catalytically inert. Nevertheless, many of these "pseudokinase" proteins are expressed and have been demonstrated to perform functions that do not involve substrate phosphorylation (Leslie, 2013). For example, a pseudo-MAPK in yeast (Mlp1) was shown to regulate transcription (Kim *et al.*, 2008) and to bind Msg5 through an unusual docking domain (Palacios *et al.*, 2011). Here we have shown that an incompletely phosphorylated form of Fus3 exists in the absence of catalytic activity and that this monophosphorylated form of the protein acts in opposition to the fully phosphorylated kinase. Given the evolutionary conservation of structurally similar MAPKs, we anticipate finding functionally similar, differentially phosphorylated MAPKs in other systems. A deeper understanding of MAPK regulation should point to new mechanisms and new therapeutic strategies to influence stimulus–response behaviors in humans.

MATERIALS AND METHODS

Experimental procedures

Strains, plasmids, and growth conditions. Standard methods were used throughout for growth, maintenance, and transformation of yeast and bacterial cultures as well as for the manipulation of DNA. Strains and plasmids used in this study are described in Tables 1 and 2. Mutagenesis was performed using the QuikChange site-directed mutagenesis kit (Life Technologies, Grand Island, NY). Yeast strains carrying integrated mutations were constructed using the *Delitto Perfetto* method (Storici *et al.*, 2001). Oligonucleotides used for strain construction and DNA amplification of *FUS3* T180 and Y182 mutants are listed in Table 3. Cells were grown in synthetic complete medium, absent specific nutrients to maintain plasmid selection, and containing 2% (wt/vol) dextrose.

Strain name[a]	Genotype	Source
BY4741	*MAT***a** *leu2Δ met15Δ his3-1 ura3Δ*	Brachmann *et al.* (1998)
fus3Δ	*MAT***a** *fus3*::kanMX	Invitrogen
msg5Δ	*MAT***a** *msg5*::kanMX	Invitrogen
ptp2/3Δ	*MAT***a** *ptp2*::*URA3 ptp3*::kanMX	Hao *et al.* (2012)
ptp2/3Δ msg5Δ	*MAT***a** *ptp2*::*URA3 ptp3*::*LEU2 msg5*::kanMX	This study
$ste5^{ND}$	*MAT***a** $ste5^{ND}$	Hao *et al.* (2008)
$ste5^{FB}$	*MAT***a** $ste5^{FB}$	This study
$ste5^{ND}$ *msg5Δ*	*MAT***a** $ste5^{ND}$ *msg5*::kanMX	This study
ste11Δ	*MAT***a** *ste11*::kanMX	Invitrogen
ste7Δ	*MAT***a** *ste7*::kanMX	Invitrogen
$fus3^{T180A}$	*MAT***a** $fus3^{T180A}$	This study
$fus3^{Y182F}$	*MAT***a** $fus3^{Y182F}$	This study
$fus3^{T180A/\ Y182F}$	*MAT***a** $fus3^{T180A/\ Y182F}$	This study

[a]All mutant strains derived from BY4741.

TABLE 1: Strains used in this study.

Transcriptional reporter and halo assay. Growth arrest (halo) and *FUS1*-LacZ levels were measured after treatment with mating pheromone, α-factor, as described previously (Hoffman *et al.*, 2002). Cells grown to $A_{600\ nm} \approx 0.8$ were stimulated for 90 min and then lysed, and β-galactosidase activity was measured spectrophotometrically after 60 min. Results are from two or three independent experiments of three or four colonies per strain read in quadruplicate.

Cell extracts and immunoblotting. Protein extracts were produced by glass bead lysis in trichloroacetic acid as previously described (Hao *et al.*, 2007). Protein concentration was determined by Dc protein assay (Bio-Rad Laboratories, Hercules, CA). Protein extracts were resolved by standard SDS–PAGE or 50 μM Mn^{2+}-Phos-tag in 10% acrylamide SDS–PAGE according to manufacturer's instructions (Wako Chemicals, Richmond, VA). Proteins were detected by immunoblotting with phospho-MAPK p44/42 antibodies (9101; Cell Signaling Technology, Beverly, MA) at 1:500, Fus3 antibodies (sc-6773, Santa Cruz Biotechnology, Dallas, TX) at 1:500, and glucose-6-phosphate dehydrogenase (G6PDH) antibodies (A9521; Sigma-Aldrich, St. Louis, MO) at 1:50,000. Immunoreactive species were visualized by fluorescence detection (Typhoon Trio+ Imager; GE Healthcare, Piscataway, NJ) of horseradish peroxidase–conjugated antibodies (sc-2006; Santa Cruz Biotechnology) at 1:10,000 using ECL-plus reagent (Life Technologies). Band intensity was quantified by scanning densitometry using ImageJ (National Institutes of Health, Bethesda, MD). Fus3 intensity values were first normalized to

slope and EC_{50} for each strain. Results are reported as ±SEM ($n = 3$). (C) Pheromone-induced growth arrest for cells treated with α-factor. Halo diameters are quantified for all strains at 5 μg (left). Results are reported as ±SEM ($n = 4$). Right, representative halo assays for the wild-type and $ste5^{ND}$ *msg5Δ* strains at 1.5, 5, and 15 μg. (D) Polarized growth in cells treated with 300 nM α-factor. Representative images for wild-type, *msg5Δ*, $ste5^{ND}$, and $ste5^{ND}$ *msg5Δ* cells, each bearing the integrated polar cap marker Bem1-GFP (arrow), at the indicated times. The path of the polar cap was quantified for 10 cells 45–200 min after pheromone addition. Data are representative of two or more experiments. Scale bar, 10 μM.

Plasmid name	Description	Source
pRS316	*CEN URA3* vector	Sikorski and Hieter (1989)
pRS316-FUS3	*CEN URA3 FUS3*	Hao *et al.* (2012)
pRS316-FUS3-T180A	*CEN URA3* $FUS3^{T180A}$	This study
pRS316-FUS3-Y182F	*CEN URA3* $FUS3^{Y182F}$	This study
pRS316-FUS3-T180A/Y182F	*CEN URA3* $FUS3^{T180A/Y182F}$	This study
pRS425-FUS1-lacZ	2 μ *LEU2* P_{FUS1}-lacZ	Hoffman *et al.* (2002)

All plasmids used in Figure 1.

TABLE 2: Plasmids used in this study.

G6PDH loading control, and values for nonphosphorylated, monophosphorylated, and dual-phosphorylated bands were calculated as a percentage of the total for each lane. To capture changes in Fus3 protein induction over time and/or between different genetic backgrounds, samples were normalized to the 15-min time point. Briefly, the value of total Fus3 in the 15-min lane served as the denominator for calculating values of the three Fus3 forms at all time points. When comparing wild-type and mutant strains, all lanes were normalized to the 15-min time point of wild type.

Microscopy. Cells expressing Bem1-GFP were examined in a microfluidic device as previously described (Kelley *et al.*, 2015) in the presence of 300 nM pheromone. This was carried out on an Olympus IX83 with an Andor Revolution XD spinning disk unit. Images were taken every 5 min as a *z*-series of 1-μm step size, 5 μm around the focal plane. These images were aligned in FIJI (fiji.sc/Fiji) using the Descriptor-based series registration (2D/3D + t) plug-in. A single-pixel Gaussian blur was applied to the fluorescence images to remove camera noise, and a maximum intensity projection was created of the stacks. To plot the polar cap path, the Bem1-GFP images were thresholded to determine the centroid of the polar cap. The centroids were recorded for each time point for every cell from 0 to 200 min. Using MATLAB, the Cartesian coordinates of the polar cap centroids were converted to polar coordinates, and each path was rotated such that the final 50 min of time points had an average angle of 0. The first 45 min of experimental data was not included in the analysis to exclude data from mitotic events. The normalized paths were converted back into Cartesian coordinates and smoothed with the "smooth" function in MATLAB, using a window size of seven time points. Ten individual paths were plotted for each strain.

Primer name	Sequence
P1 Fus3-CORE 60up	TTA GCA AGA ATC ATT GAC GAG TCA GCC GCG GAC AAT TCA GAG CCC ACA GGT CAG CAA AGC GGC GAG CTC GTT TTC GAC ACT GG
P2 Fus3-CORE 60dn	CAC GTC CAT GGC CCT TGA GTA TTT GGC AGA GGT TAA CAT CAC CTC TGG CGC CCT GTA CCA ACG TCC TTA CCA TTA AGT TGA TC
P1 Fus3 activation-loop IRO	CCA GAT GCT GAG TGA CGA
P2 Fus3 activation-loop IRO	GCA GGG TAC ATG GGA AGC

TABLE 3: Oligonucleotides used in this study.

Mathematical model

We tested three different processive models for the time-dependent behavior of Fus3 activity. The models differ in the mechanism by which Ste5 negatively regulates Fus3 activity. The first model assumes that feedback-phosphorylated Ste5 (pSte5m) has no effect on the Fus3 phosphorylation rate. The second model assumes that pSte5m has no effect on the Fus3 dephosphorylation rate. The third model combines the effect of pSte5m on phosphorylation of npFus3 and dephosphorylation of ppFus3 and pFus3 and contains the other two models as limiting cases. We describe this model in detail and point out how the other two were obtained from it. We explicitly modeled the temporal evolution of three species of Ste5: 1) free and inactive (Ste5c), 2) plasma membrane bound and active (Ste5m), and 3) feedback-phosphorylated, plasma membrane bound, and less active (pSte5m). We assumed that the total population of Ste5 is conserved and that Ste5 is recruited to the plasma membrane upon stimulation with mating pheromone. The model assumed that Fus3 is dually phosphorylated in a processive manner. To test whether feedback phosphorylation of Ste5 affects the activation of Fus3, we assumed that the rate of Fus3 phosphorylation depends on the form of Ste5 (Ste5m or pSte5m) with which Fus3 is associated. We assumed that Fus3 is induced and degraded and that monophosphorylated (pFus3) or dual-phosphorylated (ppFus3) Fus3 feedback-phosphorylates Ste5m. We modeled Fus3 dephosphorylation as a distributive process. We assumed that the dephosphorylation rate depends on the current level of the induced dual-specificity phosphatase Msg5. Because the mechanism by which Ste5 limits Fus3 activity is not known, we also included the possibility that dephosphorylation rate depends on the phosphorylated Ste5 species (pSte5m).

The equations that describe the evolution of Ste5 species are as follows:

$$\frac{d[\text{Ste5m}]}{dt} = k_1\text{Pheromone}[\text{Ste5c}] + k_4[\text{pSte5m}] - k_2[\text{Ste5m}] - k_3[\text{Ste5m}][\text{ppFus3}] - k_3'[\text{Ste5m}][\text{pFus3}] \quad (1)$$

$$\frac{d[\text{Ste5c}]}{dt} = k_2[\text{Ste5m}] + k_2'[\text{pSte5m}] - k_1^*\text{Pheromone}^*[\text{Ste5c}] \quad (2)$$

$$\frac{d[\text{pSte5m}]}{dt} = k_3[\text{Ste5m}][\text{ppFus3}] + k_3'[\text{ste5m}][\text{pFus3}] - k_2'[\text{pSte5m}] - k_4[\text{pSte5m}] \quad (3)$$

where the first term of Eq. 1 describes the rate at which mating pheromone induces the recruitment of Ste5 to the plasma membrane. The second term defines the dephosphorylation rate for pSte5m. The third term defines the rate at which Ste5 transitions back to the cytosol. The fourth and fifth terms define rates of feedback phosphorylation of Ste5m by dual-phosphorylated Fus3 (ppFus3) and monophosphorylated Fus3 (pFus3), respectively. In addition, the second term in Eq. 2 defines the rate at which pSte5m returns to Ste5c.

Parameter	Complete model	Limiting case 1	Limiting case 2	Description
k_1	1.15×10^{1}	8.51	7.71	[Ste5m] activation
k_2	1.25×10^{-4}	1.12×10^{-4}	2.43×10^{-2}	[Ste5m] deactivation
k_{2p}	1.66×10^{-2}	1.1×10^{-4}	2.43×10^{-2}	[pSte5m] deactivation
k_3	$(2.73 \times 10^{-4}, 4.09 \times 10^{-5})$	$(1.18 \times 10^{-4}, 1.77 \times 10^{-5})$	$(1.5 \times 10^{-4}, 2.25 \times 10^{-5})$	[Ste5m] feedback phosphorylation
k_{3p}	$(4.81 \times 10^{-2}, 7.21 \times 10^{-3})$	$(1.43 \times 10^{-2}, 2.15 \times 10^{-3})$	$(4.78 \times 10^{-2}, 7.17 \times 10^{-3})$	[Ste5m] feedback phosphorylation
k_b	1.29×10^{-4}	8.2×10^{-2}	2.55×10^{-3}	[Fus3] dephosphorylation
k_4	4.36×10^{-1}	4.38×10^{-1}	4.88×10^{-1}	[p-Ste5m] dephosphorylation
k_5	1.15	1.48	1.32	[Fus3] synthesis
k_{5p}	0.0	0.0	0.0	
k_6	2.64×10^{-3}	2.49×10^{-3}	3.26×10^{-3}	[Fus3] degradation
k_7	1.43×10^{-1}	1.46×10^{-1}	1.94×10^{-1}	[pp-Fus3] phosphorylation
k_{7p}	9.13×10^{-2}	1.46×10^{-1}	7.73×10^{-1}	[pp-Fus3] feedback phosphorylation
k_8	6.01×10^{-4}	6.71×10^{-4}	0.0	[pp-Fus3] dephosphorylation
k_9	1.16×10^{-3}	1.64×10^{-3}	0.0	[p-Fus3] dephosphorylation
k_{10}	5.19×10^{-4}	1.06×10^{-3}	1.14×10^{-3}	[Fus3] synthesis
k_{11}	5.16×10^{-3}	4.06×10^{-4}	3.28×10^{-3}	[Msg5] synthesis
k_{12}	1.09×10^{-4}	5.39×10^{-4}	1.11×10^{-4}	[Msg5] degradation
k_{ms}	$(2.04 \times 10^{-3}, 0.)$	$(3.19 \times 10^{-3}, 0.)$	$(2.82 \times 10^{-4}, 0.)$	[Msg5] dephosphorylation
k_{amsg5}	1.06×10^{-4}	2.16×10^{-2}	1.09×10^{-4}	[Msg5] activation
K_1	2.5×10^{-1}	2.45×10^{1}	2.47×10^{1}	Michaelis constant
K_2	3.1	1.31×10^{1}	2.84	Michaelis constant
K_3	4.12	1.04	1.03	Michaelis constant
K_4	1.07	2.49×10^{1}	1.16	Michaelis constant
K_{msg5}	1.62	1.36	2.71	Michaelis constant

The name, numerical value, and function of each rate parameter in the model are given. The rate parameters k_3 and k_{3p} are shown for the wild-type (left), *ste5*ND (right), and *msg5*Δ plus *ste5*ND (right) models. The rate parameter k_{ms} is shown for the wild-type (left) and *msg5*Δ plus *ste5*ND (right) models. Parameters k_3 and k_{3p} are "knocked down" in the model and are assumed to take 5% of the original value for both the *ste5*ND and *ste5*ND plus *msg5*Δ mutant models. Parameter k_{ms} is set to 0 for both the *msg5*Δ and *ste5*ND plus *msg5*Δ mutant models. Parameters k_{5p} and K_2 have no appreciable affect on the model and are set to 0 in the model figures.

TABLE 4: Model rate parameters.

The equation that describes the evolution of the nonphosphorylated Fus3 (npFus3) concentration is

$$\frac{d[\text{npFus3}]}{dt} = k_{10} + \frac{k_5[\text{ppFus3}]}{K_1 + [\text{ppFus3}]} + \frac{k_5'[\text{pFus3}]}{K_2 + [\text{pFus3}]} + (k_{ms}[\text{Msg5}] + k_9[\text{pSte5m}] + k_b)[\text{pFus3}] - \frac{k_7[\text{Ste5m}][\text{npFus3}]}{K_3 + [\text{npFus3}]} - \frac{k_7'[\text{pSte5m}][\text{npFus3}]}{K_4 + [\text{npFus3}]} - k_6[\text{npFus3}] \quad (4)$$

The first term on the right-hand side of Eq. 4 accounts for basal induction of Fus3. The second and third terms correspond to the positive feedback resulting from induction of Fus3 via ppFus3 and pFus3, respectively. Positive-feedback follows Michaelis–Menten kinetics, where our parameter search suggests that the rate of Fus3 induction by ppFus3 is faster than that mediated by pFus3 (see Table 4 for all parameter values). The fourth term describes the rate at which monophosphorylated Fus3 (pFus3) is dephosphorylated. We assumed three mechanisms for dephosphorylation. The first depends on the phosphatase Msg5, whose expression is induced by active Fus3. The second is independent of Msg5 and is included to test the possibility that feedback-phosphorylated Ste5 (pSte5m)

limits Fus3 activity by increasing the dephosphorylation rate (perhaps by recruiting another phosphatase). Finally, we include a basal dephosphorylation rate that is independent of Msg5 and Ste5. The fifth and sixth terms in Eq. (4) define rates of dual phosphorylation mediated by Ste5m and pSte5m, respectively. These terms allow us to test the possibility that feedback-phosphorylated Ste5 (pSte5m) limits Fus3 activity by decreasing the phosphorylation rate (i.e., $k_7' < k_7$). The last term defines the degradation rate for Fus3.

The rate equations that describe dual-phosphorylated and monophosphorylated Fus3 are

$$\frac{d[\text{ppFus3}]}{dt} = \frac{k_7[\text{Ste5m}][\text{Fus3}]}{K_3 + [\text{npFus3}]} + \frac{k_7[\text{Ste5m}][\text{Fus3}]}{K_4 + [\text{npFus3}]} - (k_{\text{ms}}[\text{Msg5}] + k_8[\text{pSte5m}] + k_{\text{b}})[\text{ppFus3}] - k_6[\text{ppFus3}] \quad (5)$$

$$\frac{d[\text{pFus3}]}{dt} = (k_{\text{ms}}[\text{Msg5}] + k_8[\text{pSte5m}] + k_{\text{b}})[\text{ppFus3}] - (k_{\text{ms}}[\text{Msg5}] + k_9[\text{pSte5m}] + k_{\text{b}})[\text{pFus3}] - k_6[\text{pFus3}] \quad (6)$$

where terms describing the rates of phosphorylation, dephosphorylation, and degradation have the same form as in Eq. 4.

The rate equation that describes evolution of the Msg5 concentration is

$$\frac{d[\text{Msg5}]}{dt} = k_{11} + \frac{k_{\text{amsg5}}[\text{ppFus3}]}{K_{\text{amsg5}}[\text{ppFus3}]} - k_{12}[\text{Msg5}] \quad (7)$$

where the first and second terms are the basal and ppFus3-dependent synthesis rates, respectively. The third term defines the rate of Msg5 degradation.

Equations 1–7 define the full model that allows for the possibility that Ste5 affects both the phosphorylation and dephosphorylation rates of Fus3. The model in which pSte5m only decreases the phosphorylation rate is obtained by setting the parameters k_8 and k_9 equal to zero, and the model in which pSte5m only increases the dephosphorylation rate is achieved by setting $k_7' = k_7$.

ACKNOWLEDGMENTS

We thank John Houser for insightful discussions about mathematical modeling strategies. This work was supported, in whole or in part, by National Institutes of Health Grants R01-GM080739 (to H.G.D.), R01-GM079271 (to T.C.E.), T32-GM067553, and R25-GM05533612 (to P.C.M.).

REFERENCES

Andersson J, Simpson DM, Qi M, Wang Y, Elion EA (2004). Differential input by Ste5 scaffold and Msg5 phosphatase route a MAPK cascade to multiple outcomes. EMBO J 23, 2564–2576.

Aoki K, Yamada M, Kunida K, Yasuda S, Matsuda M (2011). Processive phosphorylation of ERK MAP kinase in mammalian cells. Proc Natl Acad Sci USA 108, 12675–12680.

Bardwell L (2005). A walk-through of the yeast mating pheromone response pathway. Peptides 26, 339–350.

Bhattacharyya RP, Remenyi A, Good MC, Bashor CJ, Falick AM, Lim WA (2006). The Ste5 scaffold allosterically modulates signaling output of the yeast mating pathway. Science 311, 822–826.

Brachmann CB, Davies A, Cost GJ, Caputo E, Li J, Hieter P, Boeke JD (1998). Designer deletion strains derived from Saccharomyces cerevisiae S288C: a useful set of strains and plasmids for PCR-mediated gene disruption and other applications. Yeast 14, 115–132.

Breitkreutz A, Boucher L, Tyers M (2001). MAPK specificity in the yeast pheromone response independent of transcriptional activation. Curr Biol 11, 1266–1271.

Breitkreutz A, Tyers M (2006). Cell signaling. A sophisticated scaffold wields a new trick. Science 311, 789–790.

Canagarajah BJ, Khokhlatchev A, Cobb MH, Goldsmith EJ (1997). Activation mechanism of the MAP kinase ERK2 by dual phosphorylation. Cell 90, 859–869.

Chan RK, Otte CA (1982a). Isolation and genetic analysis of Saccharomyces cerevisiae mutants supersensitive to G1 arrest by a factor and a factor pheromones. Mol Cell Biol 2, 11–20.

Chan RK, Otte CA (1982b). Physiological characterization of Saccharomyces cerevisiae mutants supersensitive to G1 arrest by a factor and a factor pheromones. Mol Cell Biol 2, 21–29.

Choi KY, Satterberg B, Lyons DM, Elion EA (1994). Ste5 tethers multiple protein kinases in the MAP kinase cascade required for mating in S. cerevisiae. Cell 78, 499–512.

Dixit G, Kelley JB, Houser JR, Elston TC, Dohlman HG (2014). Cellular noise suppression by the regulator of G protein signaling Sst2. Mol Cell 55, 85–96.

Doi K, Gartner A, Ammerer G, Errede B, Shinkawa H, Sugimoto K, Matsumoto K (1994). MSG5, a novel protein phosphatase promotes adaptation to pheromone response in S. cerevisiae. EMBO J 13, 61–70.

Elion EA, Satterberg B, Kranz JE (1993). FUS3 phosphorylates multiple components of the mating signal transduction cascade: evidence for STE12 and FAR1. Mol Biol Cell 4, 495–510.

English JG, Shellhammer JP, Malahe M, McCarter PC, Elston TC, Dohlman HG (2015). MAPK feedback encodes a switch and timer for tunable stress adaptation in yeast. Sci Signal 8, ra5.

Ferrell JE Jr (2000). What do scaffold proteins really do? Sci STKE 2000, pe1.

Ferrell JE Jr, Bhatt RR (1997). Mechanistic studies of the dual phosphorylation of mitogen-activated protein kinase. J Biol Chem 272, 19008–19016.

Flatauer LJ, Zadeh SF, Bardwell L (2005). Mitogen-activated protein kinases with distinct requirements for Ste5 scaffolding influence signaling specificity in Saccharomyces cerevisiae. Mol Cell Biol 25, 1793–1803.

Garrison TR, Zhang Y, Pausch M, Apanovitch D, Aebersold R, Dohlman HG (1999). Feedback phosphorylation of an RGS protein by MAP kinase in yeast. J Biol Chem 274, 36387–36391.

Gartner A, Nasmyth K, Ammerer G (1992). Signal transduction in Saccharomyces cerevisiae requires tyrosine and threonine phosphorylation of FUS3 and KSS1. Genes Dev 6, 1280–1292.

Hao N, Behar M, Parnell SC, Torres MP, Borchers CH, Elston TC, Dohlman HG (2007). A systems-biology analysis of feedback inhibition in the sho1 osmotic-stress-response pathway. Curr Biol 17, 659–667.

Hao N, Nayak S, Behar M, Shanks RH, Nagiec MJ, Errede B, Hasty J, Elston TC, Dohlman HG (2008). Regulation of cell signaling dynamics by the protein kinase-scaffold Ste5. Mol Cell 30, 649–656.

Hao N, Yildirim N, Nagiec MJ, Parnell SC, Errede B, Dohlman HG, Elston TC (2012). Combined computational and experimental analysis reveals mitogen-activated protein kinase-mediated feedback phosphorylation as a mechanism for signaling specificity. Mol Biol Cell 23, 3899–3910.

Hao N, Yildirim N, Wang Y, Elston TC, Dohlman HG (2003). Regulators of G protein signaling and transient activation of signaling: experimental and computational analysis reveals negative and positive feedback controls on G protein activity. J Biol Chem 278, 46506–46515.

Haystead TA, Dent P, Wu J, Haystead CM, Sturgill TW (1992). Ordered phosphorylation of p42mapk by MAP kinase kinase. FEBS Lett 306, 17–22.

Hoffman G, Garrison TR, Dohlman HG (2002). Analysis of RGS proteins in Saccharomyces cerevisiae. Methods Enzymol 344, 617–631.

Huang CY, Ferrell JE Jr (1996). Ultrasensitivity in the mitogen-activated protein kinase cascade. Proc Natl Acad Sci USA 93, 10078–10083.

Hung W, Olson KA, Breitkreutz A, Sadowski I (1997). Characterization of the basal and pheromone-stimulated phosphorylation states of Ste12p. Eur J Biochem 245, 241–251.

Hur JY, Kang GY, Choi MY, Jung JW, Kim KP, Park SH (2008). Quantitative profiling of dual phosphorylation of Fus3 MAP kinase in Saccharomyces cerevisiae. Mol Cells 26, 41–47.

Kelley JB, Dixit G, Sheetz JB, Venkatapurapu SP, Elston TC, Dohlman HG (2015). RGS proteins and septins cooperate to promote chemotropism by regulating polar cap mobility. Curr Biol 25, 275–285.

Kim KY, Truman AW, Levin DE (2008). Yeast Mpk1 mitogen-activated protein kinase activates transcription through Swi4/Swi6 by a noncatalytic mechanism that requires upstream signal. Mol Cell Biol 28, 2579–2589.

Kinoshita E, Kinoshita-Kikuta E, Takiyama K, Koike T (2006). Phosphate-binding tag, a new tool to visualize phosphorylated proteins. Mol Cell Proteomics 5, 749–757.

Kusari AB, Molina DM, Sabbagh W Jr, Lau CS, Bardwell L (2004). A conserved protein interaction network involving the yeast MAP kinases Fus3 and Kss1. J Cell Biol 164, 267–277.
Leslie M (2013). Molecular biology. "Dead" enzymes show signs of life. Science 340, 25–27.
Levchenko A, Bruck J, Sternberg PW (2000). Scaffold proteins may biphasically affect the levels of mitogen-activated protein kinase signaling and reduce its threshold properties. Proc Natl Acad Sci USA 97, 5818–5823.
Maeder CI, Hink MA, Kinkhabwala A, Mayr R, Bastiaens PI, Knop M (2007). Spatial regulation of Fus3 MAP kinase activity through a reaction-diffusion mechanism in yeast pheromone signalling. Nat Cell Biol 9, 1319–1326.
Mahanty SK, Wang Y, Farley FW, Elion EA (1999). Nuclear shuttling of yeast scaffold Ste5 is required for its recruitment to the plasma membrane and activation of the mating MAPK cascade. Cell 98, 501–512.
Maleri S, Ge Q, Hackett EA, Wang Y, Dohlman HG, Errede B (2004). Persistent activation by constitutive Ste7 promotes Kss1-mediated invasive growth but fails to support Fus3-dependent mating in yeast. Mol Cell Biol 24, 9221–9238.
Malleshaiah MK, Shahrezaei V, Swain PS, Michnick SW (2010). The scaffold protein Ste5 directly controls a switch-like mating decision in yeast. Nature 465, 101–105.
Palacios L, Dickinson RJ, Sacristan-Reviriego A, Didmon MP, Marin MJ, Martin H, Keyse SM, Molina M (2011). Distinct docking mechanisms mediate interactions between the Msg5 phosphatase and mating or cell integrity mitogen-activated protein kinases (MAPKs) in Saccharomyces cerevisiae. J Biol Chem 286, 42037–42050.
Parnell SC, Marotti LA Jr, Kiang L, Torres MP, Borchers CH, Dohlman HG (2005). Phosphorylation of the RGS protein Sst2 by the MAP kinase Fus3 and use of Sst2 as a model to analyze determinants of substrate sequence specificity. Biochemistry 44, 8159–8166.
Piala AT, Humphreys JM, Goldsmith EJ (2014). MAP kinase modules: the excursion model and the steps that count. Biophys J 107, 2006–2015.
Printen JA, Sprague GF Jr (1994). Protein-protein interactions in the yeast pheromone response pathway: Ste5p interacts with all members of the MAP kinase cascade. Genetics 138, 609–619.
Remenyi A, Good MC, Bhattacharyya RP, Lim WA (2005). The role of docking interactions in mediating signaling input, output, and discrimination in the yeast MAPK network. Mol Cell 20, 951–962.
Roberts CJ, Nelson B, Marton MJ, Stoughton R, Meyer MR, Bennett HA, He YD, Dai H, Walker WL, Hughes TR, *et al.* (2000). Signaling and circuitry of multiple MAPK pathways revealed by a matrix of global gene expression profiles. Science 287, 873–880.
Segall JE (1993). Polarization of yeast cells in spatial gradients of alpha mating factor. Proc Natl Acad Sci USA 90, 8332–8336.
Sikorski RS, Hieter P (1989). A system of shuttle vectors and yeast host strains designed for efficient manipulation of DNA in Saccharomyces cerevisiae. Genetics 122, 19–27.
Storici F, Lewis LK, Resnick MA (2001). In vivo site-directed mutagenesis using oligonucleotides. Nat Biotechnol 19, 773–776.
Takahashi S, Pryciak PM (2008). Membrane localization of scaffold proteins promotes graded signaling in the yeast MAP kinase cascade. Curr Biol 18, 1184–1191.
van Drogen F, Stucke VM, Jorritsma G, Peter M (2001). MAP kinase dynamics in response to pheromones in budding yeast. Nat Cell Biol 3, 1051–1059.
Wang Y, Dohlman HG (2004). Pheromone signaling mechanisms in yeast: a prototypical sex machine. Science 306, 1508–1509.
Zhan XL, Deschenes RJ, Guan KL (1997). Differential regulation of FUS3 MAP kinase by tyrosine-specific phosphatases PTP2/PTP3 and dual-specificity phosphatase MSG5 in Saccharomyces cerevisiae. Genes Dev 11, 1690–1702.